

Short Communication

CuSn(OH)₆ Nanocubes as High-Performance Anode Materials for Lithium-Ion Batteries

Zhaofu Zhou¹, Tian Chen¹, Jianqiu Deng^{1,*}, Qingrong Yao¹, Zhongmin Wang¹, Huaiying Zhou^{2,*}

¹ School of Materials Science and Engineering, Guilin University of Electronic Technology
Guangxi, Guilin 541004, China

² Guangxi Key Laboratory of Information Materials, Guilin University of Electronic Technology
Guangxi, Guilin 541004, China

* E-mail: jqdeng@guet.edu.cn, zhy@guet.edu.cn,

Received: 8 October 2017 / Accepted: 17 December 2017 / Published: 28 December 2017

Nanostructured CuSn(OH)₆ cubes with a particle size distribution of 20-1140 nm as anode materials for lithium-ion batteries were prepared by co-precipitation method, and their structure and morphology were characterized by XRD, SEM and TEM techniques. The galvanostatic charge/discharge tests, cyclic voltammetry (CV) and electrochemical impedance spectroscopy (EIS) methods have also been employed to investigate the electrochemical performance of CuSn(OH)₆ nanocubes. The as-obtained CuSn(OH)₆ nanocubes deliver an initial discharge capacity of 551.7 mAh g⁻¹, and retains the capacity up to 569.8 mAh g⁻¹ after 100 cycles at a current density of 100 mA g⁻¹ (0.2 C). A good rate capability of CuSn(OH)₆ nanocubes has also demonstrated by galvanostatic charge/discharge tests, indicating that the CuSn(OH)₆ nanocubes are potential anode materials for lithium-ion batteries.

Keywords: Lithium-ion batteries, Anode, CuSn(OH)₆, Nanocubes, Co-precipitation method

1. INTRODUCTION

With the rapid development of portable devices, electric vehicles, large-scale energy storage system, the application of lithium-ion batteries is increasingly extensive owing to their high energy densities, long cycle life and environmental friendliness [1-3]. Although graphite has been used in commercial lithium-ion batteries, a limited theoretical capacity (372 mAh g⁻¹) can't meet the requirement of lithium-ion batteries with high energy densities. Recently, extensive researches have been carried out on exploring alternative anode materials with much higher capacities [4, 5]. Li, Sn, Sb, Ge, and Si-based materials, with high theoretical capacity, have been explored extensively as anodes for high-performance LIBs [6-8]. Among these anode materials, Sn-based materials, such as

Sn/C composites [9], intermetallic compounds [10], tin oxide [11], tin sulfide [12, 13], and tin selenide [14], have been considered as a promising candidate because of their high theoretical specific capacity, low cost and easy fabrication. However, Sn-based materials commonly suffer from severe capacity fading due to poor kinetics and huge volume change of tin upon cycling, which limits their commercial applications. In order to improve the electrochemical performance (the capacity, cycle performance, and rate capability) of Sn-based anode materials, numerous strategies have been applied, including designing rational structure of composite materials, adopting new binder, and adding electrolyte additive [8, 15, 16].

Recently, tin-based hydroxides have been intensively investigated as anode materials for lithium-ion batteries because of their superior electrochemical performance and versatility [17-20]. For example, $\text{ZnSn}(\text{OH})_6$ [17, 18] and $\text{CoSn}(\text{OH})_6$ [19] have been reported as attractive anode materials for lithium-ion batteries. In addition, $\text{MnSn}(\text{OH})_6$ nanoparticles have acted as precursors for fabricating Sn-MnO@C nanocomposites via a simple heat treatment [20] and the ultrafine Mn_2SnO_4 nanoparticles have been prepared by thermal decomposition of precursor $\text{MnSn}(\text{OH})_6$ also with high capacity [21]. To the best of our knowledge, the synthesis, photocatalytic and antiferromagnetic behavior of $\text{CuSn}(\text{OH})_6$ has been reported [22, 23], but there are no reports on the application of $\text{CuSn}(\text{OH})_6$ as an anode material for lithium-ion batteries.

In this work, $\text{CuSn}(\text{OH})_6$ nanocubes were synthesized via a simple co-precipitation method and then used as anode materials for lithium-ion batteries. A discharge capacity of 569.8 mAh g^{-1} is retained after 100 cycles at a current density of 100 mA g^{-1} (0.2 C) in the voltage range of 0-2 V. The superior electrochemical performance of $\text{CuSn}(\text{OH})_6$ nanocubes indicates their promising application as anode materials for lithium-ion batteries.

2. EXPERIMENTAL

2.1 Synthesis of $\text{CuSn}(\text{OH})_6$ nanocubes

$\text{CuSn}(\text{OH})_6$ nanocubes were prepared by a coprecipitation method with minor modification [24]. All chemicals were of analytical purity, and were used without further purification. In a typical experiment, $\text{CuCl}_2 \cdot 2\text{H}_2\text{O}$ and sodium citrate were homogeneously mixed in 60 ml deionized water at room temperature under stirring, followed by additional 15 ml of $\text{SnCl}_4 \cdot 5\text{H}_2\text{O}$ ethanol solution (4 M). Then, a 15 ml NaOH aqueous solution (2 M) was added dropwise to the mixed solution. After stirring for 30 minutes, a light blue product was obtained by filtering and washing with water and ethanol, then drying at $80 \text{ }^\circ\text{C}$ for 12 h.

2.2 Material characterization

The phase structure and surface morphology of $\text{CuSn}(\text{OH})_6$ were investigated by X-ray diffraction technique (XRD, Xpert PLXcel^{3D}, Co $\text{K}\alpha$ radiation) and field emission scanning electron microscopy (FE-SEM, Hitachi SU-70). An energy dispersive spectrometer (EDS) was employed for

the qualitatively elemental analysis of the product. The morphology was also characterized by transmission electron microscopy (TEM) and high resolution TEM (HRTEM, JEM-1200EX, 120KV).

2.3 Electrochemical measurements

The electrochemical properties of $\text{CuSn}(\text{OH})_6$ were tested with 2032-type coin cells. The working electrodes were prepared by mixing the active material, acetylene black, and carboxymethylated cellulose (CMC) binder dissolved in a solution of citric acid at a weight ratio of 8:1:1, pasting onto pure copper foil, and then drying at 80 °C under vacuum for 10 h. The foil was punched into circular electrodes with a diameter of 14 mm. The electrolyte was a solution of 1 M LiPF_6 in ethylene carbonate (EC) and dimethyl carbonate (DMC) (1:1 by volume). Pure lithium foil was used as the counter electrode. Celgard 2325 membrane was used as the separator. 2032-type coin cells were assembled in an argon-filled glove box with concentrations of water and oxygen below 0.5 ppm. The cells were discharged/charged under 100 mA g^{-1} with a voltage window between 0.01 and 2.0 V on an Arbin testing instrument (BT-2000) at room temperature. Rate capability was also investigated under different current densities. Cyclic voltammetry (CV) and electrochemical impedance spectroscopy (EIS) were performed on a Solartron Modulab electrochemical workstation.

3. RESULTS AND DISCUSSION

The crystal structure of $\text{CuSn}(\text{OH})_6$ powders was characterized by powder XRD technique. Figure. 1 shows the XRD pattern of the as-synthesized $\text{CuSn}(\text{OH})_6$ powders. It can be clearly seen that all the diffraction peaks of the sample are indexed as a pure tetragonal $\text{CuSn}(\text{OH})_6$ (PDF No. 00-020-0369) with the space group $P4/\text{mbm}$, which is consistent with the previous results [22, 25-27]. The diffraction peaks are relatively sharp and no feature peaks for the impurities can be observed, indicating that the obtained pure $\text{CuSn}(\text{OH})_6$ has good crystallinity [17]. The crystallite size of the sample is estimated to be about 34.2 nm by the Scherrer equation using the peak at $2\theta = 27.2^\circ$. Morphology and size of $\text{CuSn}(\text{OH})_6$ were investigated by SEM and TEM. From the SEM images (Fig. 2a, b) we can see that this sample consists of nanocubes with the smooth surface. The particle sizes of the $\text{CuSn}(\text{OH})_6$ nanocubes by determined Nano Measurer software are in the range 20-1140 nm (Fig. 2c), with the main contributions of 38.7% and 41.7% coming from particles with average particle sizes of 100 nm and 300 nm, respectively. The tetragonal phase $\text{CuSn}(\text{OH})_6$ could be prepared in an aqueous solution by co-precipitation of Cu^{2+} , Sn^{4+} , and OH^- according to the equation: $\text{Cu}^{2+} + \text{Sn}^{4+} + 6\text{OH}^- \rightarrow \text{CuSn}(\text{OH})_6$. The formation of $\text{CuSn}(\text{OH})_6$ nanocubes is resulted from its intrinsic tetragonal crystal structure [24, 28]. As depicted in Fig. 2d, TEM image also confirms that the sample is composed of uniform nanocubes with an average particle size of about 165 nm, which is consistent with SEM results. The interplanar distance of 0.19 nm is revealed in high-resolution TEM (HRTEM) image (Fig. 2e), which corresponds to the (400) plane. The HRTEM and selected area electron diffraction (SAED)

images (Fig. 2f) show that the $\text{CuSn}(\text{OH})_6$ nanocubes have a crystalline structure, which is confirmed by the XRD pattern.

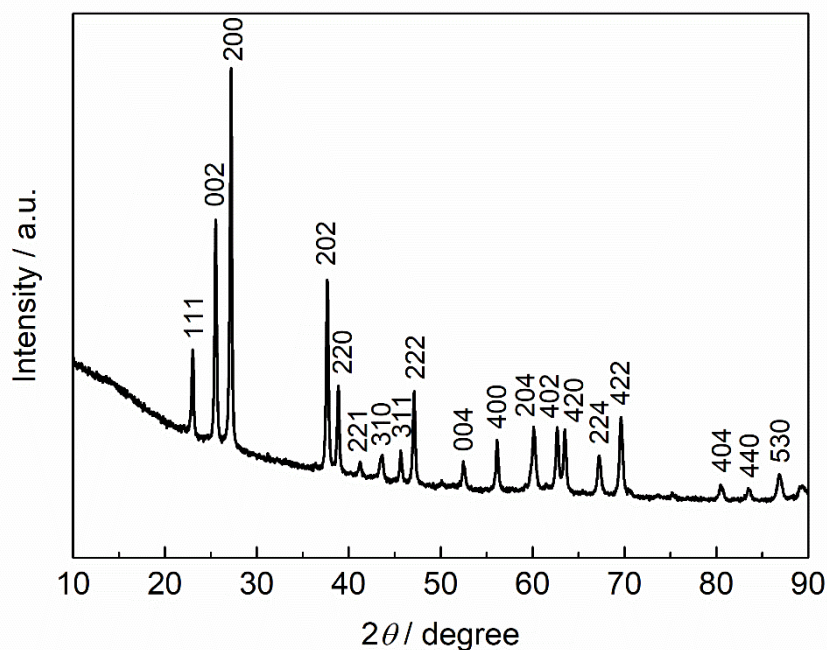
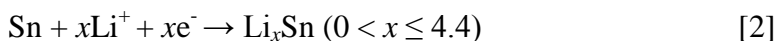
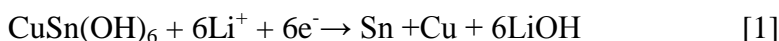


Figure 1. XRD pattern of the $\text{CuSn}(\text{OH})_6$ nanocubes.

The CV curves of $\text{CuSn}(\text{OH})_6$ sample were recorded at a scanning rate of 0.5 mV s^{-1} between 0.01 V and 2 V as shown in Figure 3a. In the first cycle, a cathodic peak appears around 1.65 V, and disappears in the following cycles, which may be attributed to the decomposition of electrolyte [27]. Another two cathodic peaks located at 1.24 and 0.16 V correspond to the decomposition of $\text{CuSn}(\text{OH})_6$ and the formation of Li_xSn alloys [29-32]. The cathodic peak near 0.03 V can be ascribed to insertion reaction of Li into acetylene black. Three anodic peaks located at about 0.60, 1.22 and 1.83 V correspond to the dealloying reaction during the anodic scan. In the second and subsequent cycles, the cathodic peaks at 1.24 and 0.16 V shift to 1.10 and 0.39 V, the anodic peaks remain unchanged. The electrochemical reactions for lithium insertion into the $\text{CuSn}(\text{OH})_6$ nanocubes are suggested as following:



The discharge/charge curves of the $\text{CuSn}(\text{OH})_6$ nanocubes at a constant current density of 100 mA g^{-1} (0.2 C) are shown in Fig. 3b. During discharge, the plateaus located at about 1.0 and 0.4 V can be observed, attributing to the multi-step Li-Sn alloy reactions. The charge plateaus at about 0.6 and 1.2 V correspond to the delithiation reaction. These plateaus are good agreement with the redox peaks in CV curves. Figure 3c presents the corresponding cycling performance. The $\text{CuSn}(\text{OH})_6$ nanocubes deliver an initial discharge capacity of 551.7 mAh g^{-1} , which is higher than that of the $\text{ZnSn}(\text{OH})_6$ nanocubes at 100 mA g^{-1} (286.5 mAh g^{-1}) [33]. In the subsequent cycles, the capacity decreases firstly and then increases gradually. After the 50th cycle, the discharge capacity reaches the maximum (626.5

mAh g⁻¹), then the capacity slowly fades to 569.8 mAh g⁻¹ over 50 cycles. Compared to previously reported the similar materials, e.g., 310 mAh g⁻¹ at 500 mA g⁻¹ for ZnSn(OH)₆ nanocubes [18], and 218 mAh g⁻¹ at 100 mA g⁻¹ for CoSn(OH)₆ [19], the CuSn(OH)₆ nanocubes display higher specific capacities and better cycling stability.

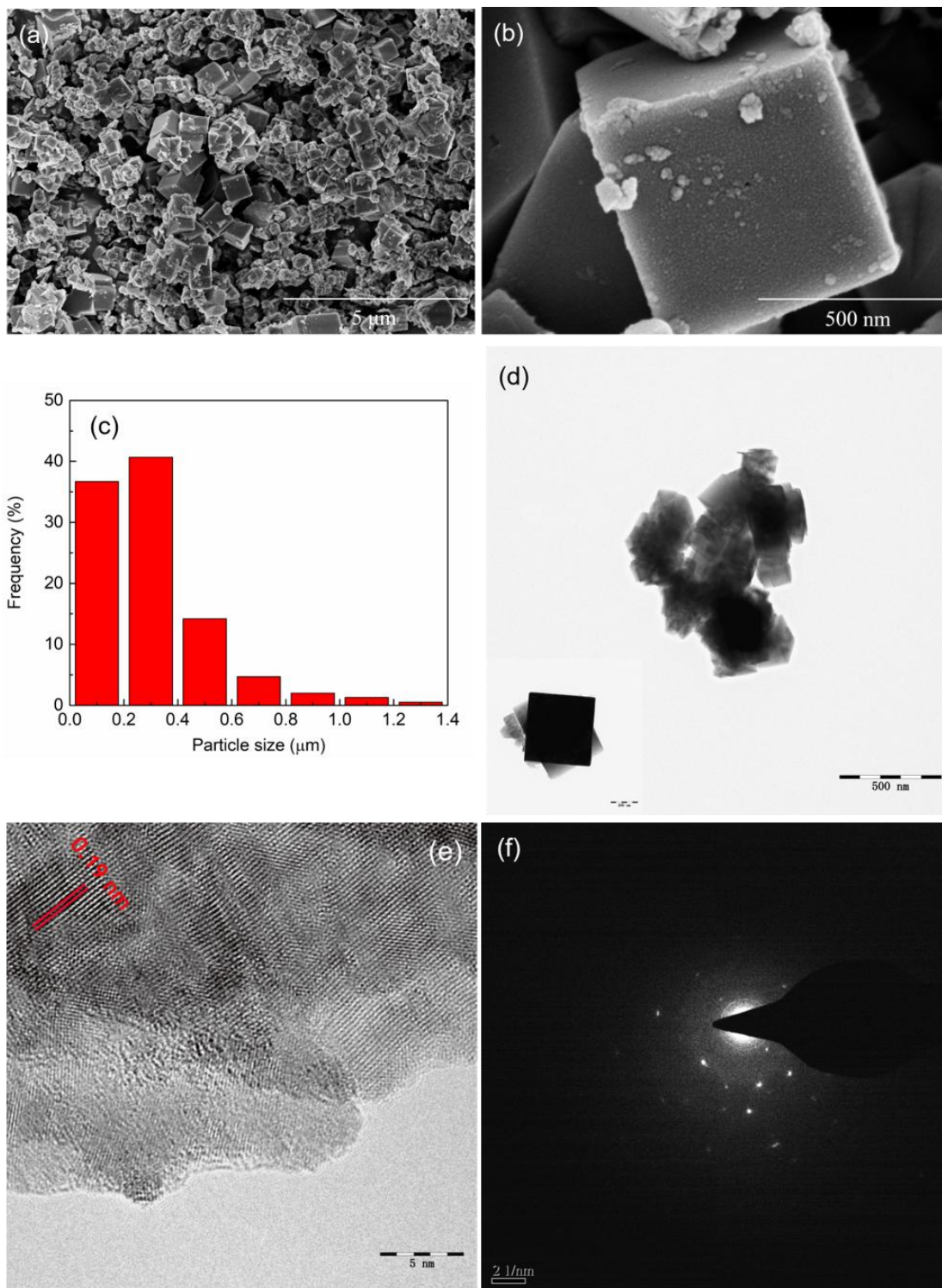


Figure 2. SEM and TEM images of CuSn(OH)₆ nanocubes. (a, b) SEM images, (c) Particle size distribution, (d) TEM image, (e) HRTEM image, (f) SAED image.

The good cyclability of the $\text{CuSn}(\text{OH})_6$ electrodes implies that LiOH can effectively buffer the volume change during charge/discharge process [19]. The evolution of capacity may be attributed to the electrochemical activity of the Sn-based electrode, which is gradually increased during discharge-charge cycling due to the volume expansion/contraction of Sn, leading to the slow impregnation of the solvated electrolyte into the active materials.

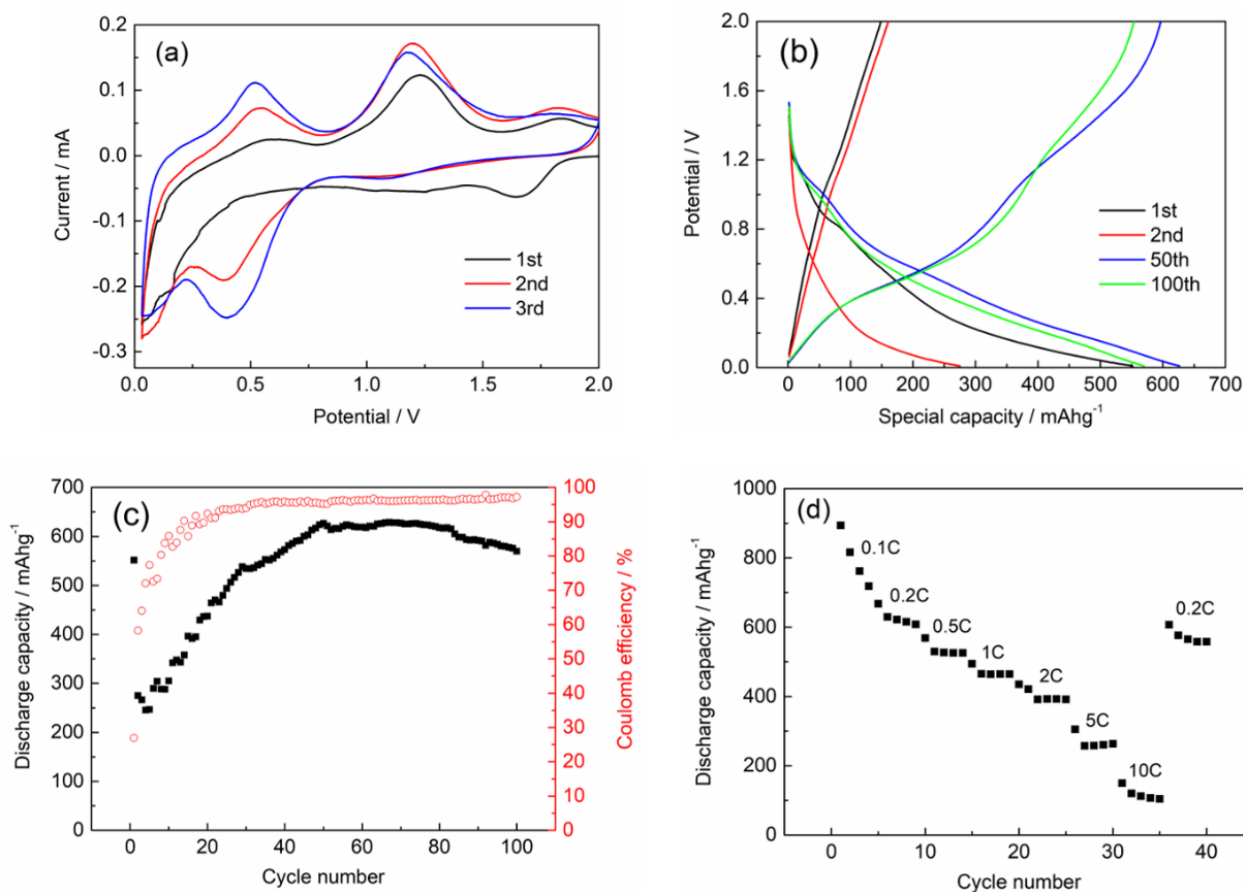


Figure 3. Electrochemical performance of $\text{CuSn}(\text{OH})_6$ nanocubes. (a) CV curves at a rate of 0.5 mV s^{-1} , (b) Discharge/charge curves at 100 mA g^{-1} (0.2 C), (c) Cycling performance at 100 mA g^{-1} , (d) Rate capability.

From Fig. 3d, the discharge capacity decreases from 894.1 to 150 mAh g^{-1} with the increasing current densities from 0.1 C to 10 C ($1 \text{ C} = 500 \text{ mA g}^{-1}$). The discharge capacity could recover to 606.8 mAh g^{-1} when the current density returns to 0.2 C , indicating the good rate and cycling performance of the $\text{CuSn}(\text{OH})_6$ nanocubes as anode materials for LIBs. To the best of our knowledge, the initial large irreversible capacity is almost inevitable for most reported anode materials. In this experiment, the capacity loss in the first cycle might be mainly attributed to the irreversible reduction of the active materials, the electrolyte decomposition [17], which is consistent with the CV curves. These results indicate that the $\text{CuSn}(\text{OH})_6$ nanocubes have superior electrochemical performance compared to many reported Sn-based anodes (Table 1).

Table 1. Comparison of electrochemical performance of various reported Sn-based anodes.

Materials	Cycling stability	Rate capacity	Reference
Hollow ZnSn(OH) ₆ nanospheres	801.2 mAh g ⁻¹ after 60 cycles at 100 mA g ⁻¹ 741.9 mAh g ⁻¹ after 1000 cycles at 1000 mA g ⁻¹	603 mAh g ⁻¹ at 1000 mA g ⁻¹	[17]
The ZnSn(OH) ₆ nanocube–graphene composite	540 mAh g ⁻¹ after 40 cycles at 500 mA g ⁻¹	469.4 mAh g ⁻¹ at 2000 mA g ⁻¹	[18]
CoSn(OH) ₆ hybridized with anionic and cationic graphenes	1475 mAh g ⁻¹ after 100 cycles at 100 mA g ⁻¹	860 mAh g ⁻¹ at 1000 mA g ⁻¹	[19]
Cubic ZnSn(OH) ₆	286.5 mAh g ⁻¹ after 30 cycles at 100 mA g ⁻¹	-	[33]
CuSnO ₃	640 mAh g ⁻¹ after 20 cycles	-	[34]
carbon-coated CaSnO ₃ nanotubes	150 mAh g ⁻¹ after 30 cycles at 60 mA g ⁻¹	-	[35]
ZnSnO ₃ -C hollow microcubes	703 mAh g ⁻¹ after 50 cycles at 100 mA g ⁻¹	287 mAh g ⁻¹ at 1000 mA g ⁻¹	[36]
Solid ZnSnO ₃ microcubes	189 mAh g ⁻¹ after 50 cycles at 100 mA g ⁻¹	-	
CoSnO ₃ @C nanoboxes	450 mAh g ⁻¹ after 400 cycles at 200 mA g ⁻¹	310 mAh g ⁻¹ at 1000 mA g ⁻¹	[37]
CuSn(OH) ₆ nanocubes	626.5 mAh g ⁻¹ after 50 cycles at 100 mA g ⁻¹ 569.8 mAh g ⁻¹ after 100 cycles at 100 mA g ⁻¹	149.9 mAh g ⁻¹ at 5000 mA g ⁻¹	This work

Electrochemical impedance spectroscopy (EIS) was also applied to explore the kinetic behaviors of the CuSn(OH)₆ anodes. The amplitude of the signal was kept at 5 mV and the frequency range of measurement was 100 KHz to 10 mHz. Impedance spectrum of the anode after 100 galvanostatic discharge-charge cycles was fitted by using the Zview 3.3 software, as shown in Figure 4. The impedance spectrum is composed of depressed semicircles and a straight sloping line. The high-frequency depressed semicircles are assigned to SEI layer impedance (R_f) and the charge-transfer resistance (R_{ct}) [38, 39]. The sloping line arises from the Warburg impedance (Z_w) owing to the diffusion of Li ions in the materials. The value of charge-transfer resistance is 116.2 Ω , indicating rapid transport of charged species, as well as good rate performance.

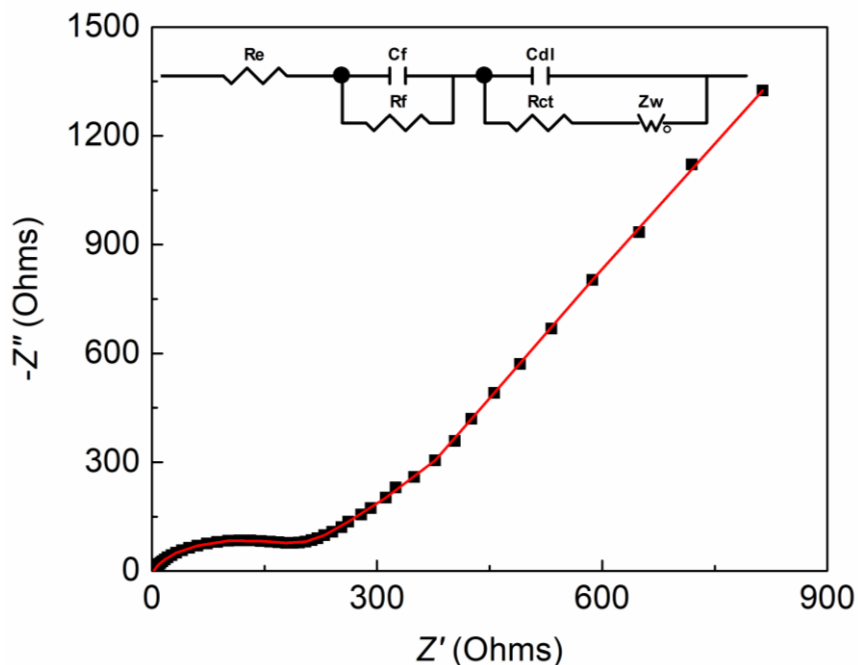


Figure 4. Nyquist plot the CuSn(OH)_6 nanocubes after 100 galvanostatic discharge-charge cycles.

4. CONCLUSION

In summary, CuSn(OH)_6 nanocubes have been synthesized via a facile co-precipitation method. The high crystalline and nanocube structure are confirmed by XRD, SEM and TEM techniques. CuSn(OH)_6 nanocubes as anode materials for lithium-ion batteries show high capacities, good cycling and rate performance. An initial discharge capacity is 551.7 mAh g^{-1} , and retains 569.8 mAh g^{-1} after 100 cycles at a current density of 100 mA g^{-1} (0.2 C) in the voltage range of $0\text{-}2 \text{ V}$. The superior electrochemical performance demonstrates that CuSn(OH)_6 nanocubes are promising anode materials for lithium-ion batteries.

ACKNOWLEDGMENTS

This work was funded by the National Natural Science Foundation of China (No. 51661009 and 21363005) and Innovation Project of GUET Graduate Education (No. 2016YJXC01).

References

1. D. Deng, *Energy Sci. Eng.*, 3 (2015) 385-418.
2. G.E. Blomgren, *J. Electrochem. Soc.*, 164 (2017) A5019-A5025.
3. N. Nitta, F. Wu, J.T. Lee and G. Yushin, *Mater. Today*, 18 (2015) 252-264.
4. S. Ji, L. Yu, X. Xu, L. Zhang and J. Liu, *Mater. Res. Bull.*, 96 (2017) 28-34.
5. J. Liu, M. Gu, L. Ouyang, H. Wang, L. Yang and M. Zhu, *ACS Appl. Mater. Inter.*, 8 (2016) 8502-8510.
6. J. Chen, *Materials*, 6 (2013) 156-183.
7. N. Nitta and G. Yushin, *Part. Part. Syst. Char.*, 31 (2014) 317-336.

8. W. Li, X. Sun and Y. Yu, *Small Methods*, 1 (2017) 1600037 (1-22).
9. Y. Xu, Q. Liu, Y. Zhu, Y. Liu, A. Langrock, M.R. Zachariah and C. Wang, *Nano Lett.*, 13 (2013) 470-474.
10. X.-L. Wang, W.-Q. Han, J. Chen and J. Graetz, *ACS Appl. Mater. Inter.*, 2 (2010) 1548-1551.
11. Y.C. Lu, C. Ma, J. Alvarado, T. Kidera, N. Dimov, Y.S. Meng and S. Okada, *J. Power Sources*, 284 (2015) 287-295.
12. T.-J. Kim, C. Kim, D. Son, M. Choi and B. Park, *J. Power Sources*, 167 (2007) 529-535.
13. B. Luo, Y. Fang, B. Wang, J. Zhou, H. Song and L. Zhi, *Energ. Environ. Sci.*, 5 (2012) 5226-5230.
14. J. Choi, J. Jin, I.G. Jung, J.M. Kim, H.J. Kim and S.U. Son, *Chem. Commun.*, 47 (2011) 5241-5243.
15. S. Xun, X. Song, V. Battaglia and G. Liu, *J. Electrochem. Soc.*, 160 (2013) A849-A855.
16. Z. Yang, A.A. Gewirth and L. Trahey, *ACS Appl. Mater. Inter.*, 7 (2015) 6557-6566.
17. R. Zhang, Y. He and L. Xu, *J. Mater. Chem. A*, 2 (2014) 17979-17985.
18. C. Chen, X. Zheng, J. Yang and M. Wei, *Phys. Chem. Chem. Phys.*, 16 (2014) 20073-20078.
19. S.J. Richard Prabakar, S.C. Han, J. Jeong, K.-S. Sohn and M. Pyo, *Mater. Design*, 118 (2017) 294-303.
20. L. Fan, Y. Zhu, J. Zhang, J. Liang, L. Wang, D. Wei, X. Li and Y. Qian, *Electrochim. Acta*, 121 (2014) 21-26.
21. S. Lei, K. Tang, C. Chen, Y. Jin and L. Zhou, *Mater. Res. Bull.*, 44 (2009) 393-397.
22. S.-L. Zhong, R. Xu, L. Wang, Y. Li and L.-F. Zhang, *Mater. Res. Bull.*, 46 (2011) 2385-2391.
23. D. Huang, X. Fu, J. Long, X. Jiang, L. Chang, S. Meng and S. Chen, *Chem. Eng. J.*, 269 (2015) 168-179.
24. Z. Wang, Z. Wang, H. Wu and X.W. Lou, *Sci. Rep-UK*, 3(3) (2013) 1391.
25. J.W. Kramer, B. Kelly and V. Manivannan, *Cent. Eur. J. Chem.*, 8 (2010) 65-69.
26. P. Villars and K. Cenzual, Springer Berlin Heidelberg, pp. (2012) 77-77.
27. K. T. Liao, Doctoral Dissertations. America, (2013)195.
28. L. Wang, K. Tang, Z. Liu, D. Wang, J. Sheng and W. Cheng, *J. Mater. Chem.*, 21 (2011) 4352-4357.
29. X. Fan, X. Tang, D. Ma, P. Bi, A. Jiang, J. Zhu and X. Xu, *J. Solid State Electrochem.*, 18 (2014) 1137-1145.
30. S. Wang, W. Zhao, Y. Wang, X. Liu and L. Li, *Electrochim. Acta*, 109 (2013) 46-51.
31. W.X. Lei, Y. Pan, Y.C. Zhou, W. Zhou, M.L. Peng and Z.S. Ma, *RSC Adv.*, 4 (2014) 3233-3237.
32. S. Chen, Y. Xin, Y. Zhou, F. Zhang, Y. Ma, H. Zhou and L. Qi, *J. Mater. Chem. A*, 2 (2014) 15582-15589.
33. X. Guo, M. Cai, R. Li and X. Han, *CrystEngComm*, 18 (2016) 6608-6613.
34. T. Liu, R.B. Du and X.J. Kong, *Adv. Mater. Res.*, 535-537 (2012) 31-35.
35. X. Hu, T. Xiao, W. Huang, W. Tao and B. Heng, *Appl. Surf. Sci.*, 258 (2012) 6177-6183.
36. Q. Xie, Y. Ma, X. Zhang, H. Guo, A. Lu, L. Wang, G. Yue and D. Peng, *Electrochim. Acta*, 141 (2014) 374-383.
37. Z. Wang, Z. Wang, W. Liu, W. Xiao and W.L. Xiong, *Energ. Environ. Sci.*, 6 (2013) 87-91.
38. J. Chen, L. Yang, S. Fang, Z. Zhang and S.-i. Hirano, *Electrochim. Acta*, 105 (2013) 629-634.
39. D. Zhou, W.L. Song, X. Li, L.Z. Fan and Y. Deng, *J. Alloy. Compd.*, 699 (2016) 730-737.